Park, J., Lühr, H., Min, K. W., Lee, J.-J. (2010): Plasma density undulations in the nighttime mid-latitude F-region as observed by CHAMP, KOMPSAT-1, and DMSP F15. - Journal of Atmospheric and Solar-Terrestrial Physics, 72, 2-3, 183-192

DOI: 10.1016/j.jastp.2009.11.007

Plasma density undulations in the nighttime mid-latitude F-region as observed by CHAMP, KOMPSAT-1, and DMSP F15

Jaeheung Park[a,b], Hermann Lühr[a], Kyoung Wook Min[b], Jae-Jin Lee[c]

[a] *Helmholtz Center Potsdam (GFZ), Sect. 2.3, Telegrafenberg, D-14473 Potsdam, Germany.*

[b] *Department of Physics, Korea Advanced Institute of Science and Technology (KAIST), Yuseong-gu, Daejeon 305-701, Republic of Korea.*

[c] *Solar and Space Weather Research Group, Korea Astronomy and Space Science Institute (KASI), Yuseong-gu, Daejeon 305-348, Republic of Korea.*

Abstract

We investigate plasma density undulations in the nighttime mid-latitude topside F-region. During solar maximum years the undulations are found at CHAMP, KOMPSAT-1, and DMSP F15 altitudes. The occurrence rate is higher at KOMPSAT-1 than at DMSP F15 altitude. The undulations occur infrequently during equinoxes, and the occurrence peaks are in the Asian/Oceanian (eastern Pacific/American) region during June (December) solstice. At CHAMP altitude the undulations are observed all through the night, and the occurrence rate is anti-correlated with the solar cycle. As all these results are in general agreement with known climatology of MSTIDs, we suggest that the undulations are a topside signature of MSTIDs. The undulations are often but not always accompanied by magnetic signatures indicating the presence of field-aligned current (FAC). The partial lack in correspondence might be due to the ionospheric conductivity variation. The similar distribution is, however, in support of a connection between density

undulations and FACs.

Key words: Ionospheric irregularities, Mid-latitude ionosphere, Topside ionosphere, Ionospheric current

1. Introduction

The mid-latitude ionospheric F-region is known to be relatively calm compared to the equatorial region where equatorial plasma bubbles (EPBs) frequently occur or the high-latitude region where auroral precipitation and polar cap convection generate complex current and plasma structures. However, though relatively weak, the mid-latitude F-region also possesses plasma structures. Plasma density irregularities in the nighttime mid-latitude F-region were first reported by *Peterson et al.* (1955). They conducted scatter-sounding experiments at the west coast of the United States, and observed echoes which were notably different from ground scattering. Those echoes were aligned with the geomagnetic field lines at the ionospheric E- and F-layer. They were generally accompanied by sporadic E (E_s) patches, but the occurrence rate had little connection with the geomagnetic activity. *Peterson et al.* (1955) suggested that the echoes originate from equatorward extension of the auroral oval. Afterwards, a number of papers were published on the topic. Using radio scintillation data above Australia, *Munro* (1963) found discrete patches of scintillation regions in the nighttime mid-latitude ionosphere. *Dyson* (1968) investigated ionograms recorded by the Alouette-I satellite, and found that the occurrence rate of topside spread F above Australia reached its maximum around June solstice.

Behnke (1979) reported band structures in the nighttime mid-latitude F region using the Arecibo incoherent scatter radar. They had horizontal widths of about 100 km, and drifted southwestward. Afterwards, such band structures were called medium-scale traveling ionospheric disturbances (MSTIDs). Using airglow images and total electron content (TEC) data at Arecibo, *Garcia et al.* (2000) found that most MSTIDs are aligned from northwest to southeast and drift southwestward. *Shiokawa et al.* (2003a) showed that the MSTID occurrence rate in the eastern Asian longitude sector maximizes during June solstice. *Otsuka et al.* (2004) and *Shiokawa et al.* (2005) found that airglow images of MSTIDs taken at geomagnetic conjugate points exactly mirror each other. *Saito et al.* (1995) observed electric and magnetic fluctuations in the nighttime mid-latitude ionospheric F region, and attributed them to mid-latitude plasma irregularities. *Shiokawa et al.* (2003b) supported the close relationship between MSTIDs and electromagnetic fluctuations by conjugate observations of airglow intensity and in-situ E-field measurements by a DMSP satellite. Recently, *Park et al.* (2009a) reported linearly-polarized magnetic field fluctuations in the nighttime mid-latitude F region, and related them to MSTIDs.

There is a consensus that MSTIDs are connected with the Perkins instability (*Perkins*, 1973) whose growth rate, γ_P, is approximately given by (*Tsunoda*, 2006):

$$\gamma_P = \frac{E_0 \; sin(\theta - \alpha) \; sin\alpha \; cosI}{BH} \tag{1}$$

where E_0 is the ambient electric field, B magnetic field strength, H neutral density scale height, θ the polarization angle of the ambient E-field measured from magnetic east, and α the polarization angle of the wave normal of the perturbed band structure. But, this equation cannot explain all the MSTID features to full satisfaction. For example, *Kelley and Makela* (2001) had to assume a finite MSTID size along the wavefront in order to reconcile the observed MSTID drift (southwestward in the northern hemisphere) with the Perkins instability theory. The linear growth rate of the Perkins instability is too small to explain the plasma density structure (e.g. *Saito et al.* (1998) and *Shiokawa et al.* (2003b)). *Shiokawa et al.* (2003b) argued that the effect of conjugate F-region and E-regions has to be considered for reconciling the disagreement. *Tsunoda and Cosgrove* (2001) and *Tsunoda* (2006) suggested that E_s and MSTIDs give positive feedback to each other through electrodynamic coupling. Recently, *Yokoyama et al.* (2009) conducted the first 3D computer simulation of the coupled E_s/Perkins instability. The directional preference of MSTID wavefronts and phase velocities was explained in terms of E_s-MSTID coupling.

Various plasma undulation phenomena in the mid-latitude nighttime F region, i.e. field-aligned irregularities (FAIs), mid-latitude spread F (MSF) and MSTIDs are closely connected with each other. *Fukao et al.* (1991) reported that FAIs are generally collocated with strong MSFs. According to *Bowman* (1992) mid-latitude spread F (MSF) is generated by tilted isodensity contours which in turn originate from MSTIDs. *Saito et al.* (2001) showed that FAIs do not always occur together with MSTIDs. *Shiokawa et al.* (2003a) reported that only 10-15% of MSTIDs were accompanied by MSFs while their statistical properties are similar. *Kotake et al.* (2006) argued that different scale sizes of the two phenomena might lead to such discrepancy. Lately, *Otsuka et al.* (2009) showed that intense FAIs occur in the plasma depletion region of MSTIDs, where enhanced gradient drift instabilities are suspected to generate FAIs. In this study we will mainly deal with MSTIDs whose scale size is several hundred kilometers.

Though there have been a lot of studies on the mid-latitude plasma structures, their full global/seasonal occurrence pattern is not known yet. Most of the previous investigations were constrained to ground observations: radar experiments (*Saito et al.*, 1998), 630.0 nm airglow imaging (*Garcia et al.*, 2000; *Otsuka et al.*, 2004; *Candido et al.*, 2008), and GPS/TEC measurements (*Kotake et al.*, 2006, 2007; *Lee et al.*, 2008). *Kotake et al.* (2006) explored the global MSTID climatology using worldwide GPS networks, but their results are restricted to the landmasses. This lack of global data coverage is because MSTID is basically a phenomenon at the bottomside ionosphere (*Saito et al.*, 2001) and there are only a few satellites orbiting at such a low altitude (below 350 km). However, some plasma density undulations do exist also in the topside ionosphere. For example, *Seker et al.* (2009) showed that MSTIDs can affect the topside as well as the bottomside ionosphere by combining airglow imager and incoherent scatter radar observations. *Livneh et al.* (2009) reported that the Arecibo incoherent scatter radar found plasma density undulations from 160 km to altitudes higher than 500 km. Also, a few groups investigated the midlatitude plasma structures by means of topside satellite observations. *Hanson and Johnson* (1992) found mid-latitude ionospheric disturbances below 300 km, which were morphologically similar to EPBs, using Atmosphere Explorer E satellite measurements. *Shiokawa et al.* (2003b) gave one example of plasma density undulation observed by DMSP F15 at 840 km altitude. Recently *Onishi et al.* (2009) observed a daytime

MSTID with DEMETER satellite (650 km altitude). The MSTID showed quasi-periodic modulation of plasma density and field-aligned flow, and were collocated with similar GPS/TEC variations. *Earle et al.* (2006) studied topside ionograms from the ISS-b satellite, and constructed for the first time a global MSF statistics. However, the observation period was only from August 1978 to December 1980, i.e. near solar maximum, and the global data coverage was poor during June solstice. *Su et al.* (2006) investigated mid-latitude irregularities of in-situ plasma density as observed by ROCSAT-1 (at 600 km altitude). They found that the irregularities generally appear in different longitude sectors in the two solstices. The occurrence rate showed a broad maximum centered at midnight, and was anti-correlated with the solar cycle. Yet, as the orbit inclination angle of ROCSAT-1 was low ($40°$), the satellite did not reach the latitude of the irregularities at all longitudes. *Saito et al.* (1995) and *Park et al.* (2009a) presented the global distributions of electric and magnetic fluctuations, respectively, associated with MSTIDs. However, their results might be different from true MSTID climatology because other factors than the plasma distribution, such as ionospheric conductivity levels, can affect the electromagnetic signals.

In this study we will investigate the plasma density undulations in the topside nighttime midlatitude F-region as observed by three satellites: CHAMP, KOMPSAT-1, and DMSP F15. As each satellite has global coverage at different altitudes, we can give the global climatology of the plasma density undulations at several altitudes as well as the solar-cycle dependence. In Section 2 we briefly describe the instruments and event detection approach. Section 3 shows the global climatology of mid-latitude plasma density undulations, which are discussed in detail in Section 4. Finally, the results are summarized in Section 5.

2. Observations

The Challenging Mini-Satellite Payload (CHAMP) was launched in July 2000 with the orbit inclination angle of 87.3°. The precession period of the orbit through 12 hours in local time is about 131 days. Right after the launch its orbit altitude was about 450 km, but slowly decreased to around 300 km as of 2009. Onboard CHAMP a Flux-Gate magnetometer (FGM) and a scalar Overhauser Magnetometer (OVM) measure the geomagnetic field, and a Planar Langmuir Probe (PLP) monitors the plasma density. After preprocessing the data rate of FGM and OVM (PLP) is 1s (15s). These three payloads are still in full operation as of June 2009, and all the data are open for public use (http://isdc.gfz-potsdam.de/index.php).

The Korea Multi-Purpose Satellite-1 (KOMPSAT-1) was launched in 1999. Its orbit is circular at 685 km altitude and sun-synchronous at 1050-2250 LT. A scientific payload, Ionospheric Measurement Sensor (IMS), has a Langmuir Probe (LP) and an Electron Temperature Probe (ETP) (*Lee et al.*, 2002). The LP measures electron density and temperature with a temporal resolution of 4s. The ETP samples the electron temperature each second. The IMS operated with a duty cycle of about 30% from the end of June 2000 to the beginning of August 2001.

The Defense Meteorological Satellite Program (DMSP) F15 is in a sun-synchronous orbit (0930-2130 LT) at the altitude of 840 km. It was launched in 1999, and has a Special Sensors-Ions, Electrons, and Scintillation (SSIES) to measure the ion density, temperature, drift, and composition. The nominal data sample period is 4s, and the duty cycle is almost 100%.

Figure 1(a)-(b) gives an example of mid-latitude plasma density undulations as observed by CHAMP. In panel (a) the thick solid line represents the plasma density, n, measured by CHAMP/PLP, and the thin dashed line is n_0, the plasma density low-pass filtered by a median filter (T_c=52s). The undulation amplitude is defined as $|n - n_0|$, which is plotted in panel (b) as a thick solid line. Near the geomagnetic equator (from $-10°$ to $+15°$) we can see equatorial plasma bubble (EPBs), whose undulation amplitudes reach well beyond $1 \times 10^5\ cm^{-3}$. On the other hand, in the southern mid-latitude region (from $-40°$ to $-25°$) there exist quasi-periodic undulations with smaller amplitudes (about $3 \times 10^4\ cm^{-3}$).

Figure 1(c)-(e) shows another example encountered by KOMPSAT-1. In panel (c) the original and low-pass-filtered plasma densities are given in the same format as in panel (a), and panel (d) represents electron temperature. Again, panel (e) is the undulation amplitude as in panel (b). Between $20° \sim 40°$ MLAT the plasma density shows quasi-periodic variations, and the electron temperature is nearly anti-correlated with it. The undulation amplitude of the plasma density is about $1.5 \times 10^4\ cm^{-3}$ as shown in panel (e).

In Figure 1(f)-(g) is an example observed by DMSP F15. In panel (f) the original and low-pass-filtered plasma densities are given in the same format as in panel (a), and panel (g) is the undulation amplitude as panel (b). The plasma density shows quasi-periodic variations between $-40° \sim -20°$ MLAT.

In this study we search for such plasma density undulations automatically based on the following procedure. First, we gather nighttime satellite passes during magnetically quiet times ($K_p < 3.7$) and apply a low-pass median filter (window size≈100s) to the plasma density. Second, if the undulation with respect to the filtered data is larger than a certain threshold ($8 \times 10^3\, cm^{-3}$), it is considered as an event. However, an event should be surrounded by calm background (undulation amplitude $< 4 \times 10^3\, cm^{-3}$) at each end for at least 30s. In this way adjacent events are tied together to be one large event. Third, to exclude EPBs and subauroral density troughs (e.g. *Yizengaw et al.* (2005)), CHAMP events are neglected when their center points are outside $\pm 20° \sim 40°$ MLAT. Considering the field-aligned geometry of the ionospheric F-region features, the latitude window is shifted equatorward to $\pm 17° \sim 37°$ MLAT for KOMPSAT-1 and DMSP F15. Events lasting shorter than 60s (about 470 km), which might originate from data outliers, are also discarded. Finally, as CHAMP/FGM continuously measures the geomagnetic field strength, we imposed an additional criterion on the CHAMP/PLP events. *Stolle et al.* (2006) reported that the magnetic field strength shows deflections inside EPBs. In order to exclude EPBs we neglected plasma density undulations within which an EPB was detected by an approach similar to that in *Stolle et al.* (2006) (high-pass filtered/rectified $|\Delta B|$ (T_c=30s) exceeds 0.2 nT). For details, the readers are referred to *Stolle et al.* (2006) and *Park et al.* (2009b). The mid-latitude plasma irregularities detected by the above-mentioned procedure are marked by a horizontal bar in Figures 1(b), 1(e), and 1(g). On the other hand, the region marked by a series of 'A' in Figure 1(e), which also shows electron density/temperature undulations above the threshold between $\pm 17° \sim 37°$ MLAT, was excluded automatically from our statistics due to its short length. In the subsequent sections we will concentrate on the events identified by the automatic procedure described above.

3. Results

Figure 2 shows the seasonal occurrence rate of mid-latitude density undulations as observed by CHAMP during the period common with KOMPSAT-1/LP: 28 June 2000 - 31 July 2001 (hereafter 'KOMPSAT-1/LP lifetime' for simplicity). Within each geographic bin (5° in latitude by 10° in longitude) the occurrence rate is calculated as the ratio between the number of detected events to the number of satellite passes over this bin. The final global image is filtered by a 3-by-3 2D median filter so that outliers are suppressed. Note that events whose center point lies outside $\pm 20° \sim 40°$ MLAT were automatically neglected. Global occurrence patterns in each season are given in panels (a)-(c), and panel (d) shows the occurrence rate as a function of invariant latitude versus local time.

First, it is noted that the occurrence rate of undulations are lowest during equinoxes. Second, the occurrence maximum during June solstice is in the Asian/Oceanian region, while it is in the eastern Pacific/American region during December solstice. In general, the occurrence rate is higher in the summer hemisphere. Third, the undulations are spread over the night, as can be seen in panel (d), with a weak maximum near midnight.

Figure 3 has the same format as Figure 2, but it is based on KOMPSAT-1/LP observations. From panels (a)-(c) we can see again that the undulations are rare during the equinoxes, and that the occurrence peaks in the

Asian/Oceanian (eastern Pacific/American) region during June (December) solstice. The occurrence rate during June solstice is higher in the summer (i.e. northern) hemisphere. While the same trend is expected for December solstice, the observed occurrence rate is not higher in the summer (i.e. southern) hemisphere. However, we should keep in mind that during December solstice the operation of KOMPSAT-1/LP in the southern hemisphere was generally limited to equatorward of $-30°$ GLAT (see Figure 2 of *Kim et al.* (2006) for reference). In panel (d) the event occurrence is confined to 22-23 LT due to the sun-synchronous orbit characteristic of KOMPSAT-1.

The same detection procedure was applied to DMSP F15 data during the KOMPSAT-1/LP lifetime, and the result is shown in Figure 4. Similar to Figures 2 and 3, the occurrence rate of the events is lowest during equinoxes, and has a weak local maximum in the Asian/Oceanian (eastern Pacific/American) region around June (December) solstice, with the peak in the summer hemisphere. Generally, the occurrence rate is lower than at the KOMPSAT-1 altitude.

Figure 5 shows the event distribution obtained from CHAMP data, but this time during the two-year solar minimum period, 2006 and 2007. During that time much more events are detected. Again, the undulation occurrence rate attains its minimum during equinoxes. During June solstice the occurrence maximum is in the Asian/Oceanian region and the minimum in the eastern Pacific, southern Atlantic, and southern African region as in Figure 2(b). The occurrence peak during December solstice is spread across the southern Pacific Ocean with the maximum above the American continent. Just like for solar maximum (Figure 2), the undulations occur through all the night, as seen in Figure 4(d), with a broad maximum shortly before midnight.

4. Discussions

4.1. statistical properties of nighttime topside mid-latitude plasma density undulations

In Section 3 we described the statistical distribution of mid-latitude plasma density undulations. During solar maximum years, CHAMP (around 400 km altitude), KOMPSAT-1 (around 680 km), and DMSP F15 (around 840 km) found similar longitudinal distribution patterns: an occurrence maximum in Asia/Oceania (eastern Pacific/American) during June (December) solstice and globally low occurrence rate during equinoxes. Unfortunately, a height-dependent relationship between the occurrence rates at CHAMP and KOMPSAT-1 altitudes is not clear from Figures 2 and 3, possibly due to different data rates: CHAMP/PLP (15s) and KOMPSAT-1/LP (4s). DMSP F15 encountered mid-latitude plasma density undulations less frequently than KOMPSAT-1. As the data rate of DMSP/SSIES is also 4s, we can conclude that the occurrence rate is higher at 680 km than at 840 km. The result is compatible with *Livneh et al.* (2009). They found plasma density undulations up to 750 km altitude using mid-latitude incoherent scatter radars, while no undulation was observed by the DMSP ion drift meter.

The undulations occur through all night at CHAMP altitude (around 400 km), and the occurrence rate is anti-correlated with the solar cycle. Also, the occurrence rate shows strong hemispheric asymmetry at CHAMP and KOMPSAT-1 altitude, i.e. preference for the summer hemisphere. The reason might be as follows. MSTIDs can be described as alternating bands which show upward/downward displacement of the F-layer (e.g. see *Tsunoda* (2006)). Let us assume a plasma instability with growth rate γ, and resultant altitude change of ionospheric F-layer, Δz, is given from Eq. (32) in *Tsunoda* (2006) as:

$$\Delta z = z - z_0 = z_0(e^{\gamma \Delta t} - 1) \tag{2}$$

where z (z_0) is perturbed (unperturbed) altitude, and Δt is elapsed time from the instability initiation. This altitude change leads to density undulation:

$$\Delta n = n - n_0 = n_0(e^{\Delta z/H_{plasma}} - 1) = n_0(e^{\frac{z_0}{H_{plasma}}(e^{\gamma \Delta t}-1)} - 1) \tag{3}$$

where n_0 is the ambient density and H_{plasma} the plasma scale height. The growth rate γ is expected to be the same in both hemispheres because the effect of an E_s-layer instability, mapped along the geomagnetic field, (rather than the Perkins instability) dominates the initial-stage growth of F-layer undulations (*Yokoyama et al.*, 2009). *Stankov and Jakowski* (2006) found from CHAMP occultation data that the plasma scale height at the topside (near CHAMP altitude) nighttime mid-latitude ionosphere is slightly lower in the summer than in the winter hemisphere. Therefore, in the topside summer hemisphere a larger background density, n_0, together with a slightly lower plasma scale height can produce larger-amplitude undulations.

Eq. (3) can also interpret the solar cycle dependence of plasma density undulations. First, scale height does not vary much with solar activity in topside (near CHAMP altitude) nighttime mid-latitude F-region (*Stankov and Jakowski*, 2006). Second, though n_0 decreases and γ increases with decreasing solar cycle (e.g. *Tsunoda* (2006)), the effect of γ, which is doubly exponential, dominates Δn. Hence, the resultant Δn is expected to become larger during solar-minimum years than during solar maximum, as confirmed by our observations shown in Figures 2 and 4.

In this paper we used a fixed threshold ($8 \times 10^3\ cm^{-3}$) to identify mid-latitude plasma density undulations. In order to assess the reliability of Figures 2-5 we also tested the relative undulation amplitude ($|n-n_0|/n_0$) for the event identification (threshold: undulation amplitude 8% of the ambient plasma density). The obtained results are generally compatible with the finding of Figures 2-5 (figures not shown). First, the event occurrence rate is generally higher at KOMPSAT-1 (680 km) than at DMSP F15 (840 km) altitude. Second, for all the three satellites the occurrence rate is lowest during equinoxes, and maximizes in the Asian/Oceanian (eastern Pacific/American) longitude sector during June (December) solstice. Third, at CHAMP altitude the density undulations occur through almost all night, but with a bias towards the post-midnight sector. Fourth, the occurrence rate is higher during solar minimum years than during solar maximum. However, the hemispheric distribution patterns show notable difference from Figures 2-5. The preference for the summer hemisphere shown in Figures 2-5 disappears when relative undulation amplitude is used for the event identification. During solar maximum CHAMP events generally appear in the winter hemisphere; the occurrence rates for KOMPSAT-1 (DMSP F15) are slightly higher in the northern (southern) hemispheres, respectively. During solar minimum the occurrence rate at CHAMP altitude is slightly higher in the southern hemisphere.

Eq. (3) predicts that the relative undulation amplitudes ($|n-n_0|/n_0$) show hemispheric symmetry if the difference in plasma scale height, H_{plasma}, can be neglected (e.g. *Stankov and Jakowski* (2006)). However, Eq. (3) cannot explain why relative density variations of CHAMP, KOMPSAT-1, and DMSP F15 data do not exhibit perfect hemispheric symmetry. It is probably related to the seasonal (hemispheric) difference of primary seeding, which originates from the neutral atmosphere. But, further investigation is needed to prove this suggestion.

4.2. comparison with other satellite observations

We want to compare the climatology given in Figures 2-4 with previous satellite observations of topside mid-latitude plasma density structures. In *Su et al.* (2006) the mid-latitude plasma density irregularities observed by ROCSAT-1 in-situ measurements occur mainly in the Asian/Oceanian (American) longitude region during June (December) solstice. The occurrence rate showed a broad maximum around midnight, and was anti-correlated with the solar cycle. All these results are consistent with ours. Yet, the number of mid-latitude plasma density irregularities encountered during equinoxes by ROCSAT-1 was comparable to that during solstices, which is slightly different from the trends shown in this paper. Mid-latitude undulations observed by ROCSAT-1 show no preference of the summer hemisphere, as seen in our Figure 2. The differences might be due to the different detection approach (i.e. relative plasma density variation) applied to ROCSAT-1 data.

According to *Earle et al.* (2006) the occurrence rate of topside MSFs, which originate from topside plasma density structures, was minimum during the spring equinox (February-April) as observed by the ISS-b satellite. The longitudinal occurrence distribution peaked in the Asian (north American) region from August to October (from November to January). Although the seasonal division is slightly different from that in this study, the results generally agree with those given in Section 3. It is noteworthy in their study that both the August-October and November-January periods show the longitudinal peaks in the northern hemisphere.

4.3. comparison with other ground observations

Next, let us compare our results with previous ground-based observations, which measure MSTIDs (i.e. plasma density structures) seen at the bottomside (by airglow imaging) or around F-region peak (by GPS/TEC measurements) in mid-latitude region. From airglow observation *Garcia et al.* (2000) reported that MSTID occurrence at Arecibo, Puerto Rico peaks during December solstice, which supports our results. The MSTID occurrence rate in the Asian/Oceanian longitude sector, estimated from airglow images, is maximum during June solstice (*Shiokawa et al.*, 2003a), which is also consistent with our results. By interpreting GPS/TEC data *Kotake et al.* (2006) also confirmed that relative nighttime MSTID amplitudes in the Asian/Oceanian and the western U. S. longitude sector are largest during June solstice. Only, in South America MSTID amplitudes were largest during June solstice, which is inconsistent with our result. From the similarities in the distribution patterns, as shown above, we suggest that topside mid-latitude plasma density undulations addressed in this paper are a topside signature (or extension) of MSTIDs.

4.4. comparison with E_s layers

The relationship between mid-latitude density undulations and E_s layers might be important because MSTID generation is promoted by E_s layers (see the theoretical works of *Tsunoda and Cosgrove* (2001); *Tsunoda* (2006); *Yokoyama et al.* (2009)). *Otsuka et al.* (2008) showed a good correlation between the observational climatologies of MSTIDs and E_s in East Asia, but there has been no such investigation on a global scale. Using CHAMP, GRACE-A, and FORMOSAT-3/COSMIC *Arras et al.* (2008) presented a global E_s climatology for the years 2006 and 2007 (see their Figures 3 and 4). Their Figure 3 shows that (1) E_s occurrence is lowest during equinoxes, (2) the occurrence prefers the summer hemisphere, (3) during June solstice the occurrence is lowest in the American and eastern Pacific region, (4) during December solstice the occurrence is lowest between the Atlantic and western Indian Ocean, and (5) there are practically no E_s layers within the South Atlantic Anomaly (SAA). All of these properties are in remarkable agreement with our results at the topside ionospheric F-layer, corroborating the close relationship between the density undulations (or MSTIDs) and E_s layers as suggested by the theoretical work of *Yokoyama et al.* (2009).

4.5. relationship to midlatitude magnetic fluctuations (MMFs)

Now, we want to discuss our results in relation with mid-latitude magnetic fluctuations (MMFs). *Park et al.* (2009a) showed MMF statistics obtained by CHAMP/FGM measurements, and concluded that MMFs are magnetic signatures of MSTIDs. The argument was supported by the seasonal/longitudinal distribution and linear polarization of MMFs. The features in Figure 2 and 4 are generally compatible with Figure 2 and 3 of *Park et al.* (2009a): few events in equinoxes and occurrence maxima over Asia/Oceania (eastern Pacific Ocean/Americas) during June solstice (December solstice). However, several differences are notable. First, the mid-latitude plasma density undulations occur throughout the night while MMFs predominantly occur in the premidnight sector. Second, the occurrence rate of the plasma density undulations is anti-correlated with the solar activity while MMF occurrence has a clear positive correlation. *Park et al.* (2009a) argued that not only MSTIDs but also ambient conditions such as ionospheric conductivity seem to influence the MMF generation. As the ionospheric conductivity constantly decreases through the night, MMF generation peaks in the premidnight sector. Also, the conductivity increases with the solar cycle, and promotes MMF generation during the solar activity.

We will investigate the relationship between the plasma density undulations and MMFs in more details. Figure 5 presents an early-night example of the mid-latitude plasma density undulations. Panel (a) shows original and filtered plasma density as in Figure 1(a), panel (b) fluctuations of the zonal magnetic field measured by CHAMP/FGM, panel (c) fluctuations of the meridional component, and panel (d) presents field-aligned current density calculated from the magnetic field deviations (*Park et al.*, 2009b). The plasma undulation event detected by our automatic procedure is marked by a series of circles in panel (a). Within the event periods we can see quasi-periodic plasma density undulations collocated with linearly polarized magnetic fluctuations in the plane perpendicular to the main geomagnetic field. The correlation coefficient between zonal and meridional fluctuations, as well as the polarization angle (measured counter-clockwise from the magnetic east direction), is noted in panel (d). Because of the good linear polarization we can calculate reliably the field-aligned current density by Ampère's law, which is plotted in panel (d) (see *Park et al.* (2009a,b) for details). We note that the plasma density and magnetic signatures exhibit hemispheric conjugacy. In panel (d) large positive (field-aligned) peaks of FAC density roughly correspond to the plasma density depletion (enhancement) regions in the northern (southern) hemisphere.

All the mid-latitude plasma density undulations detected by CHAMP/PLP are reexamined to check whether they are accompanied with MMFs. An event is identified as collocated with MMFs if filtered/rectified (T_c=10s) perpendicular B-field deflections exceed 0.45 nT within the event location (1° margin on both sides) or at the conjugate point in the opposite hemisphere (see *Park et al.* (2009a)). Altogether 683 events were identified in CHAMP data as mid-latitude plasma density undulations during KOMPSAT-1/LP lifetime. Among them 425 events are collocated with MMFs, 222 events were not, and for 36 events appropriate CHAMP/FGM data are missing. On average about 66% of the plasma undulations are collocated with MMFs. MSTIDs, whose scale sizes are several hundred kilometers, are not always collocated with other irregularities of smaller scale sizes, such as FAI (*Saito et al.*, 2001) or MSF (*Shiokawa et al.*, 2003a). Note that a high-pass filter was used here to identify MMFs (T_c=10s, i.e. scale length less than 80 km) based on the studies of *Saito et al.* (1995) and *Park et al.* (2009a). Moreover, MMF amplitude is affected by ionospheric conductivity *Park et al.* (2009a). Hence, (1) the lack of secondary instabilities generating smaller-scale irregularities on MSTIDs and (2) day-to-day variability of the conductivity might have compromised a one-to-one correspondence between plasma density undulations and MMFs. This point is worth further investigation with the upcoming *Swarm* mission, which will be equipped with higher-resolution plasma instrument as well as an ion drift meter by which the E-field can be estimated.

5. Summary

In this study we investigated plasma density undulations in the nighttime mid-latitude F-region as observed by CHAMP, KOMPSAT-1, and DMSP F15. In this way the first 'full global' climatology of topside mid-latitude undulations is given at different altitudes and different solar phases. From the results obtained we come to the following conclusions.

1. In the nighttime mid-latitude ionosphere during the solar maximum, plasma density undulations (scale size $<$ 400 km) are found at CHAMP (400 km), KOMPSAT-1 (680 km), DMSP F15 (840 km) altitudes. The event occurrence rate is higher at KOMPSAT-1 (680 km) than at DMSP F15 (840 km) altitude.
2. Mid-latitude plasma density undulations occur infrequently during equinoxes. Their occurrence peaks are in the Asian/Oceanian (eastern Pacific/American) region during June (December) solstice.
3. At CHAMP altitude (400 km) the undulations are observed all through the night, and the occurrence rate is anti-correlated with the solar cycle. All these results are in general agreement with known MSTID and E_s climatology.
4. The undulations are frequently but not always accompanied by magnetic signatures indicating the presence of field-aligned current. The partial lack in correspondence might be due to the scale-size difference in detection algorithms for the two phenomena, but more probably due

to the effect of ionospheric conductivity on FAC density. The quite similar distribution is, however, in support of a connection between density undulations and FACs.

Acknowledgements: The CHAMP mission is supported by the German Aerospace Center (DLR) in operation and by the Federal Ministry of Education (BMBF), as part of the Geotechnology Programme, in data processing. The authors gratefully acknowledge the Center for Space Sciences at the University of Texas at Dallas and the US Air Force for providing the DMSP thermal plasma data.

References

Arras, C., J. Wickert, G. Beyerle, S. Heise, T. Schmidt, and C. Jacobi (2008), A global climatology of ionospheric irregularities derived from GPS radio occultation, *Geophys. Res. Lett.*, 35, L14809, doi:10.1029/2008GL034158.

Behnke, R. (1979), F layer height Bands in the Nocturnal Ionosphere over Arecibo, *J. Geophys. Res.*, 84, 974.

Bowman, G. G. (1992), Upper atmosphere neutral-particle density variations compared with spread-F occurrence rates at locations around the world, *Ann. Geo.*, 10, 676.

Candido, C. M. N., A. A. Pimenta, J. A. Bittencourt, and F. Becker-Guedes (2008), Statistical analysis of the occurrence of medium-scale traveling ionospheric disturbances over Brazilian low latitudes using OI 630.0 nm emission all-sky images, *Geophys. Res. Lett.*, 35, L17105, doi:10.1029/2008GL035043.

Dyson, P. L (1968), Topside spread F at midlatitudes, *J. Geophys. Res.*, 73, 2441.

Earle G. D., A. M. Musumba, and J. P. McClure (2006), A global study of nighttime midlatitude topside spread echoes, *J. Geophys. Res.*, 111, A11306, doi:10.1029/2006JA011614.

Fukao, S., M. C. Kelley, T. Shirakawa, T. Takami, M. Yamamoto, T. Tsuda, and S. Kato (1991), Turbulent Upwelling of the Mid-Latitude Ionosphere, 1. Observational Results by the MU Radar, *J. Geophys. Res.*, 96(A3), 3725.

Garcia, F. J., M. C. Kelley, J. J. Makela, and C. S. Huang (2000), Airglow observations of mesoscale low-velocity traveling ionospheric disturbances at midlatitudes, *J. Geophys. Res.*, 105, 18407.

Hanson, W. B., and F. S. Johnson (1992), Lower midlatitude ionospheric disturbances and the Perkins instability, *Planet. Space Sci.*, 40, 1615.

Kelley, M. C., and J. J. Makela (2001), Resolution of the discrepancy between experiment and theory of midlatitude Fregion structures, Turbulent upwelling of the mid-latitude ionosphere, 2. Theoretical framework, *Geophys. Res. Lett.*, 28(13), 2589.

Kim, H, K. Min, J. Park, J. Lee, E. Lee, H. Kil, V. P. Kim, and S. Park (2006), Comparison of satellite measurements of the low-latitude nighttime upper ionosphere with IRI, *J. Atmos. Solar Terr. Phys.*, 68, 2107.

Kotake N., Y. Otsuka, T. Tsugawa, T. Ogawa, and A. Saito (2006), Climatological study of GPS total electron content variations caused by medium-scale traveling ionospheric disturbances, *J. Geophys. Res.*, 111, A04306, doi:10.1029/2005JA011418.

Kotake, N., Y. Otsuka, T. Ogawa, T. Tsugawa, and A. Saito (2007), Statistical study of medium-scale traveling ionospheric disturbances observed with the GPS networks in Southern California, *Earth Planets Space*, 59, 95.

Lee, J. J., K. W. Min, V. P. Kim, V. V. Hegai, K.-I. Oyama, F. J. Rich, and J. Kim (2002), Large density depletions in the nighttime upper ionosphere during the magnetic storm of July 15, 2000, *Geophys. Res. Lett.*, 29(3), 1032, doi:10.1029/2001GL013991.

Lee, C. C., Y. A. Liou, Y. Otsuka, F. D. Chu, T. K. Yeh, K. Hoshinoo, and K. Matunaga (2008), Nighttime medium-scale traveling ionospheric disturbances detected by network GPS receivers in Taiwan, *J. Geophys. Res.*, 113, A12316, doi:10.1029/2008JA013250.

Livneh, D. J., I. Seker, F. T. Djuth, and J. D. Mathews (2009), Omnipresent vertically coherent fluctuations in the ionosphere with a possible worldwide-midlatitude extent, *J. Geophys. Res.*, 114, A06303, doi:10.1029/2008JA013999.

Maruyama T., and T. Matuura (1984), Longitudinal variability of annual changes in activity of equatorial spread-F and plasma bubbles, *J. Geophys. Res.*, 89, 10903.

Munro, G. H. (1963), Scintillation of radio signals from satellites, *J. Geophys. Res.*, 68, 1851.

Onishi, T., T. Tsugawa, Y. Otsuka, J.-J. Berthelier, and J.-P. Lebreton (2009), First simultaneous observations of daytime MSTIDs over North America using GPS-TEC and DEMETER satellite data, *Geophys. Res. Lett.*, 36, L11808, doi:10.1029/2009GL038156.

Otsuka, Y., K. Shiokawa, T. Ogawa, and P. Wilkinson (2004), Geomagnetic conjugate observations of medium-scale traveling ionospheric disturbances at midlatitude using all-sky airglow imagers, *Geophys. Res. Lett.*, 31, L15803, doi:10.1029/2004GL020262.

Otsuka, Y., T. Tani, T. Tsugawa, T. Ogawa, A. Saito (2008), Statistical study of relationship between medium-scale traveling ionospheric disturbance and sporadic E layer activities in summer night over Japan, *J. Atmos. Solar Terr. Phys.*, 70, 2196.

Otsuka, Y., K. Shiokawa, T. Ogawa, T. Yokoyama, and M. Yamamoto (2009), Spatial relationship of nighttime medium-scale traveling ionospheric disturbances and F region field-aligned irregularities observed with two spaced all-sky airglow imagers and the middle and upper atmosphere radar, *J. Geophys. Res.*, 114, A05302, doi:10.1029/2008JA013902.

Park, J., H. Lühr, C. Stolle, M. Rother, K. W. Min, J.-K. Chung, Y. H. Kim, I. Michaelis, and M. Noja (2009a), Magnetic signatures of medium-scale traveling ionospheric disturbances as observed by CHAMP, *J. Geophys. Res.*, 114, A03307, doi:10.1029/2008JA013792.

Park, J., H. Lühr, C. Stolle, M. Rother, K. W. Min, and I. Michaelis, (2009b), The characteristics of field-aligned currents associated with equatorial plasma bubbles as observed by the CHAMP satellite, *submitted to Ann. Geo.*.

Perkins, F. (1973), Spread F and ionospheric currents, *J. Geophys. Res.*, 78, 218.

Peterson, A. M, O. G. Villard, Jr., Rl. L. Leadabrand, and P. B. Gallagher (1955), Regularly-observable aspect-sensitive radio reflections from ionization aligned with the earth's magnetic field and located within the ionospheric layers at middle latitudes, *J. Geophys. Res.*, 60, 497.

Saito, A., T. Iyemori, M. Sugiura, N. C. Maynard, T. L. Aggson, L. H. Brace, M. Takeda, and M. Yamamoto (1995), Conjugate Occurrence of the Electric Field Fluctuations in the Nighttime Midlatitude Ionosphere, *J. Geophys. Res.*, 100(A11), 21439.

Saito, A., T. Iyemori, L. G. Blomberg, M. Yamamoto, and M. Takeda (1998), Conjugate observations of the mid-latitude electric field fluctuations with the MU radar and the Freja satellite, *J. Atmos. Solar Terr. Phys.*, 60, 129.

Saito, A., M. Nishimura, M. Yamamoto, S. Fukao, M. Kubota, K. Shiokawa, Y. Otsuka, T. Tsugawa, T. Ogawa, M. Ishii, T. Sakanoi, and S. Miyazaki (2001), Traveling Ionospheric Disturbances Detected in the FRONT Campaign, *Geophys. Res. Lett.*, 28(4), 689.

Seker, I., D. J. Livneh, and J. D. Mathews (2009), A 3-D empirical model of F region Medium-Scale Traveling Ionospheric Disturbance bands using incoherent scatter radar and all-sky imaging at Arecibo, *J. Geophys. Res.*, 114, A06302, doi:10.1029/2008JA014019.

Shiokawa, K., C. Ihara, Y. Otsuka, and T. Ogawa (2003a), Statistical study of nighttime medium-scale traveling ionospheric disturbances using midlatitude airglow images, *J. Geophys. Res.*, 108, 1052, doi:10.1029/2002JA009491.

Shiokawa, K., Y. Otsuka, C. Ihara, T. Ogawa, and F. J. Rich (2003b), Ground and satellite observations of nighttime medium-scale traveling ionospheric disturbance at midlatitude, *J. Geophys. Res.*, 108, 1145, doi:10.1029/2002JA009639.

Shiokawa, K., Y. Otsuka, T. Tsugawa, T. Ogawa, A. Saito, K. Ohshima, M. Kubota, T. Maruyama, T. Nakamura, M. Yamamoto, and P. Wilkinson (2005), Geomagnetic conjugate observation of nighttime medium- and large-scale traveling ionospheric disturbances: FRONT3 campaign, *J. Geophys. Res.*, 110(A5), A05303, doi:10.1029/2004JA010845.

Stankov, S. M., and N. Jakowski (2006), Topside ionospheric scale height analysis and modelling based on radio occultation measurements, *J. Atmos. Solar Terr. Phys.*, 68, 134.

Stolle, C., H. Lühr, M. Rother, and G. Balasis (2006), Magnetic signatures of equatorial spread F as observed by the CHAMP satellite, *J. Geophys. Res.*, 111, A02304, doi:1029/2005JA011184.

Su, S.-Y., C. H. Liu, H. H. Ho, and C. K. Chao (2006), Distribution characteristics of topside ionospheric density irregularities: Equatorial versus midlatitude regions, *J. Geophys. Res.*, 111, A06305, doi:10.1029/2005JA011330.

Tsunoda, R. T., and R. B. Cosgrove (2001), Coupled Electrodynamics in the Nighttime Midlatitude Ionosphere, *Geophys. Res. Lett.*, 28, 4171.

Tsunoda, Roland T. (2006), On the coupling of layer instabilities in the nighttime midlatitude ionosphere, *J. Geophys. Res.*, 111, A11304, doi:10.1029/2006JA011630.

Yizengaw E., H. Wei, M. B. Moldwin, D. Galvan, L. Mandrake, A. Mannucci, and X. Pi (2005), The correlation between mid-latitude trough and the plasmapause, *Geophys. Res. Lett.*, 32, L10102, doi:10.1029/2005GL022954.

Yokoyama, T., D. L. Hysell, Y. Otsuka, and M. Yamamoto (2009), Three-dimensional simulation of the coupled Perkins and Es-layer instabilities in the nighttime midlatitude ionosphere, *J. Geophys. Res.*, 114, A03308, doi:10.1029/2008JA013789.

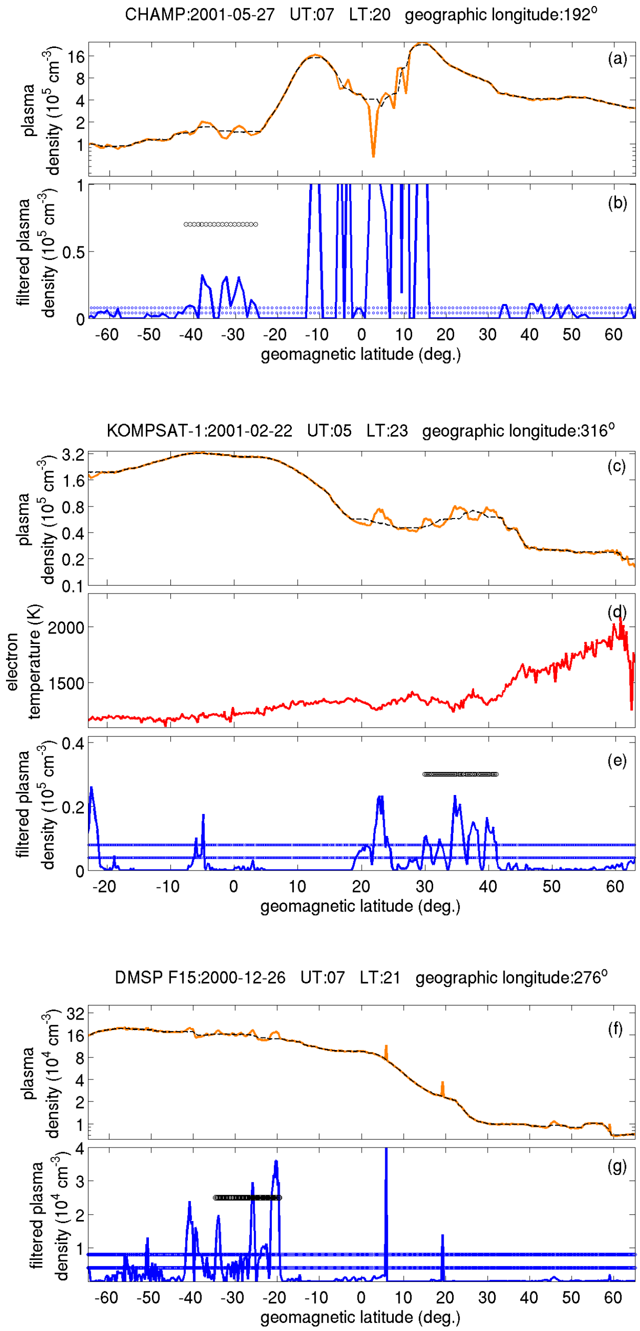

Figure 1: (a) plasma density measured by CHAMP/PLP (thick solid line) and the plasma density low-pass filtered by a median filter (thin dotted line), (b) undulation of the plasma density with respect to the low-pass filtered density, (c) plasma density measured by KOMPSAT-1/LP (thick solid line), and the plasma density low-pass filtered by a median filter (thin dotted line), (d) electron temperature measured by KOMPSAT-1/LP, (e) density undulation calculated as in panel (b), (f) plasma density measured by DMSP/SSIES (thick solid line), and the plasma density low-pass filtered by a median filter (thin dotted line), and (g) density undulation calculated as in panel (b).

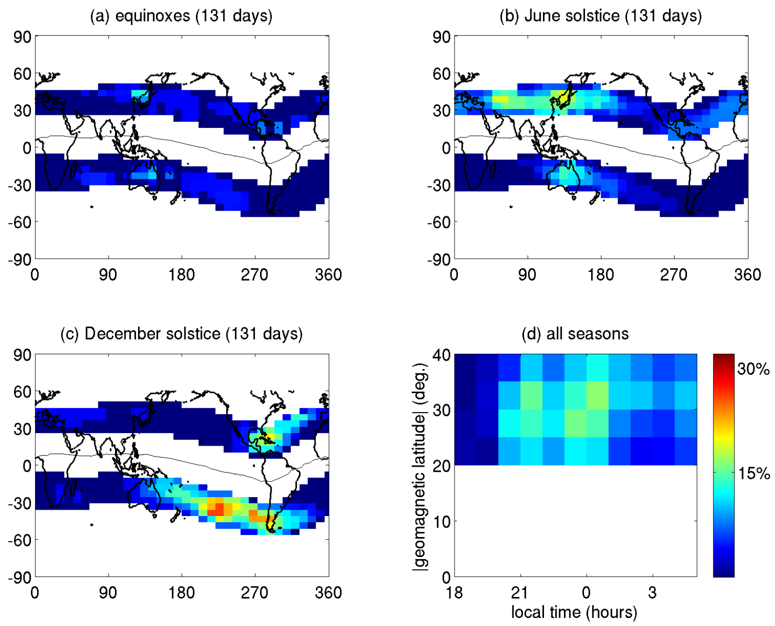

Figure 2: Seasonal/global occurrence rate of mid-latitude density undulations as observed by CHAMP during the KOMPSAT-1/LP lifetime. The distribution is presented for each season centered on: (a) equinoxes, (b) June solstice, and (c) December solstice. Panel (d) shows the occurrence rate as a function of invariant latitude versus local time.

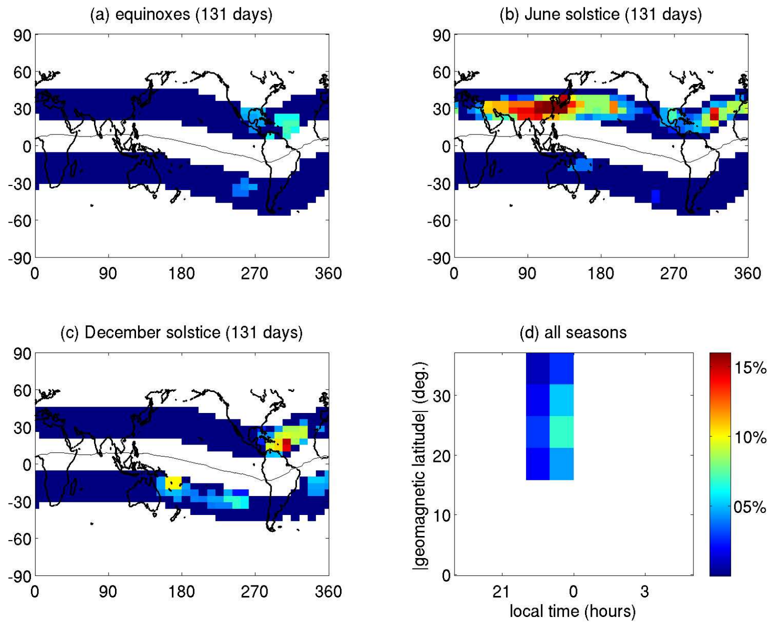

Figure 3: Same as Figure 2, but as observed by KOMPSAT-1/LP. Notice the difference in color scale.

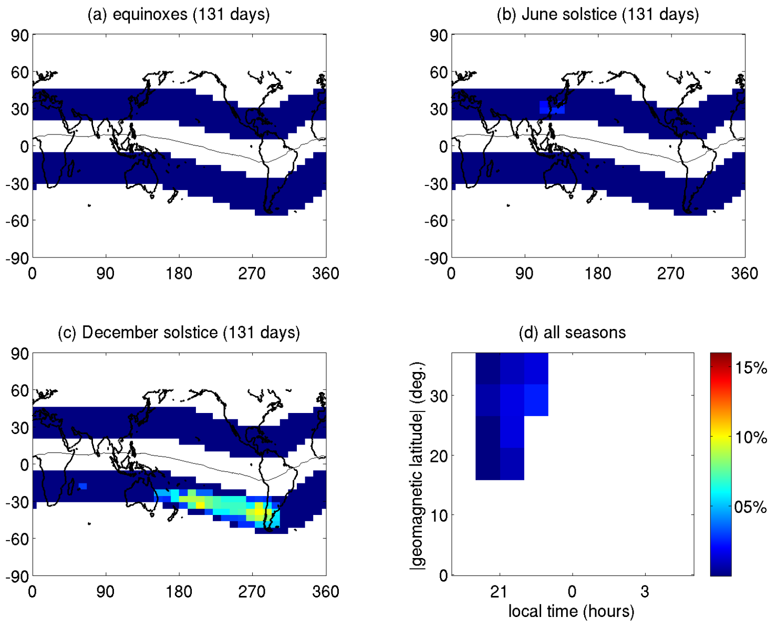

Figure 4: Same as Figure 2, but as observed by DMSP F15. Notice the difference in color scale.

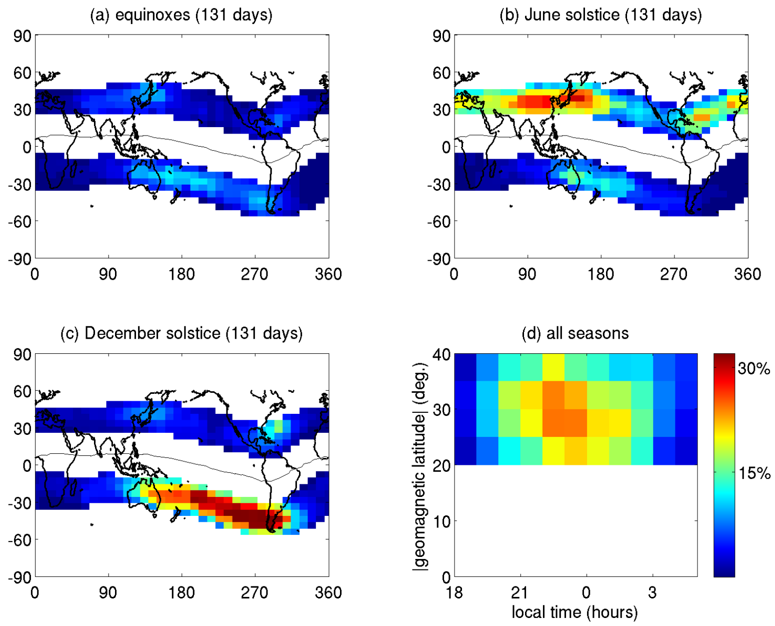

Figure 5: Same as Figure 2, but as observed by CHAMP during the years 2006 and 2007.

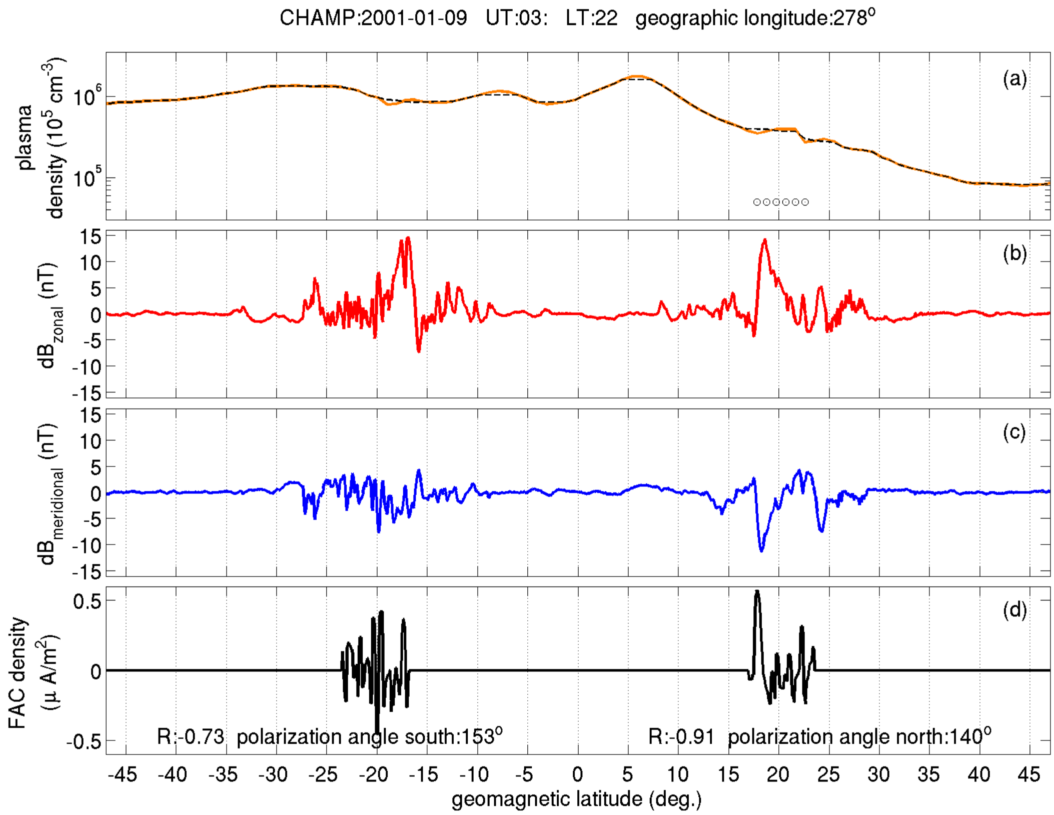

Figure 6: Comparison of density undulations with magnetic signatures. (a) plasma density measured by CHAMP/PLP (thick solid line), and the density low-pass filtered by a median filter (thin dotted line), (b) fluctuation of zonal magnetic field measured by CHAMP/FGM, (c) fluctuation of meridional comoponent, and (d) field-aligned current density calculated from the magnetic fluctuations.